

## Supporting Information

# Highly efficient plasmon-mediated electron injection into cerium oxide from embedded silver nanoparticles

Jacopo Stefano Pelli Cresi<sup>1,2</sup>, Maria Chiara Spadaro<sup>1,2</sup>, Sergio D'Addato<sup>1,2</sup>, Sergio Valeri<sup>1,2</sup>, Stefania Benedetti<sup>2</sup>, Alessandro Di Bona<sup>2</sup>, Daniele Catone<sup>3</sup>, Lorenzo Di Mario<sup>3</sup>, Patrick O'Keeffe<sup>4</sup>,  
Alessandra Paladini<sup>4</sup>, Giovanni Bertoni<sup>2,5</sup>, Paola Luches<sup>2\*</sup>

<sup>1</sup> *Dipartimento FIM, Università di Modena e Reggio Emilia, Via G. Campi 213/a, Modena, Italy*

<sup>2</sup> *CNR-NANO, Centro di Ricerca S3, via G. Campi 213/a, Modena, Italy*

<sup>3</sup> *CNR-ISM, Division of Ultrafast Processes in Materials (FLASHit), Area della Ricerca di Roma 2 Tor Vergata, Via del Fosso del Cavaliere 100, 00133 Rome, Italy.*

<sup>4</sup> *CNR-ISM, Division of Ultrafast Processes in Materials (FLASHit), Area della Ricerca di Roma 1, 00015 Monterotondo Scalo, Italy*

<sup>5</sup> *CNR-IMEM, Istituto dei Materiali per l'Elettronica ed il Magnetismo, Consiglio Nazionale delle Ricerche, Parco Area delle Scienze 37/A, 43124, Parma, Italy*

\* e-mail: [paola.luches@nano.cnr.it](mailto:paola.luches@nano.cnr.it)

## 1. HRTEM Analysis

Two representative high resolution images of the Ag NPs are shown in Figure S1. Typical reflections from (111) and (200) planes are visible, as expected from multiply twinned NPs with polyhedral shape, already observed in NPs grown with the same method.<sup>1</sup> In Figure S1a the Ag NP is oriented along the two-fold axis (FFT in the inset) and it is compatible with the McKay icosahedron with  $n = 9$  (simulation of the HRTEM image and the model at the bottom,  $n$  is the number of shells around the central atom). Figure S1b reports an Ag NP with a  $n = 12$  decahedral shape oriented along the five-fold axis (FFT in the inset) with the corresponding HRTEM simulation and the three-dimensional model at the bottom. The simulations were done using STEM\_CELL,<sup>2</sup> with a defocus value of -60 nm, after generating the atomic positions in the polyhedron with a script in MATLAB®. An amorphous ~3 nm thick slab of amorphous carbon (brown atoms in the models) was added below the Ag NPs (gray atoms) to take into account the ultrathin support film of the TEM grid.

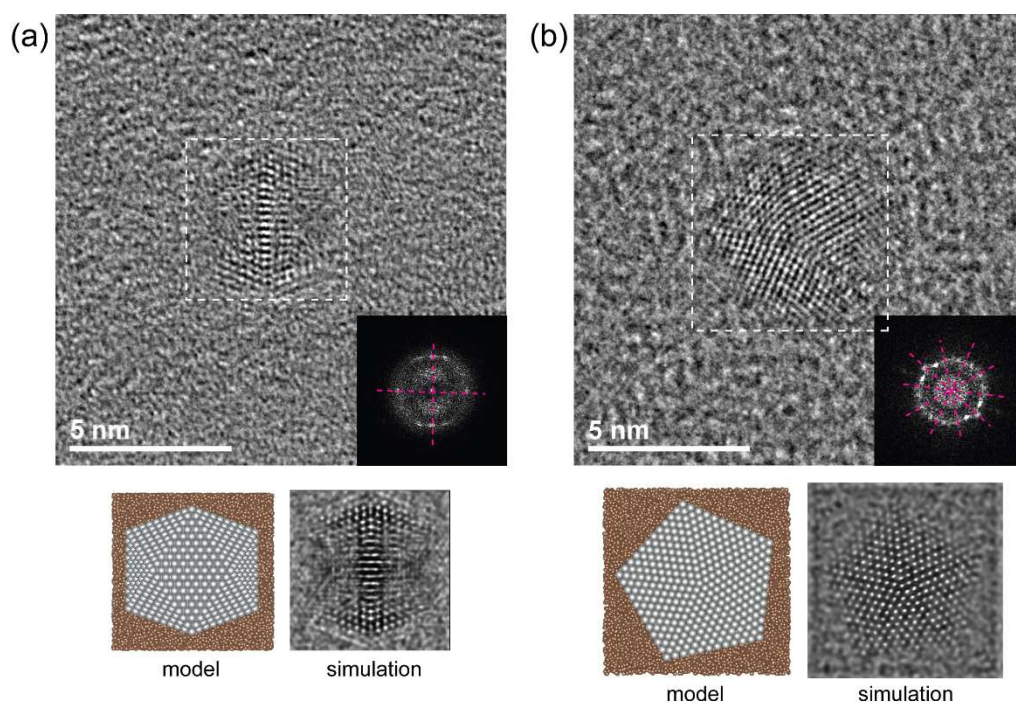


**Figure S1.** (a) HRTEM image of an Ag NP with icosahedral shape. (b) HRTEM image of an Ag NP with decahedral shape. At the bottom we show the three-dimensional model and the corresponding HRTEM simulation.

## 2. UV-Vis spectrophotometry measurements

Transmittance (T), reflectance (R) and absorbance (A) curves for the quartz substrate (green lines), for the CeO<sub>2</sub> film (blue lines) and for the Ag@CeO<sub>2</sub> sample (red lines) are shown in Figure S1. T(R) represents the ratio of the light intensity transmitted through (reflected from) the sample and the incident intensity, while A is obtained by the formula  $A=1-T-R$ . The quartz substrate does not absorb up to 275 nm. The 10 nm CeO<sub>2</sub> film spectrum shows a peak of absorbance at 300 nm and a slight absorption in visible range, possibly induced by the morphology of the CeO<sub>2</sub> film. The Ag@CeO<sub>2</sub> sample shows an additional broad absorption band in the visible ascribed to the excitation of localized surface plasmon resonances (LSPR) in the Ag NPs. From the absorbance spectra, we calculated the Tauc plot, shown in Figure S3, from which we extracted an optical band gap of  $3.44 \pm 0.03$  eV, given by the intercept between the linear extrapolation of  $(\alpha(h\nu) \cdot h\nu)^{1/2}$  and the energy axis.

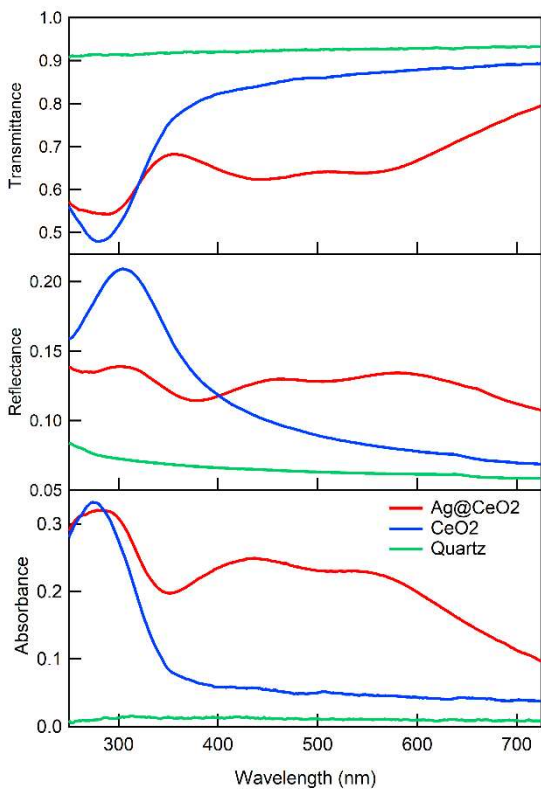


**Figure S2.** Transmittance, reflectance and absorbance spectra of the quartz, CeO<sub>2</sub> sample and Ag@CeO<sub>2</sub>.

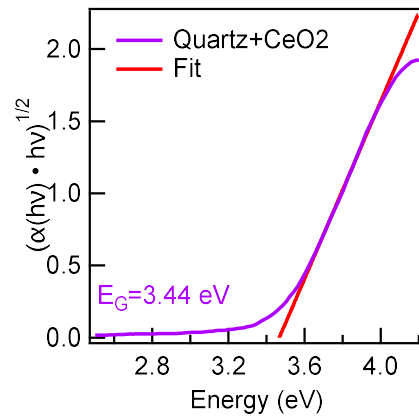


**Figure S3.** Tauc plot for the CeO<sub>2</sub> sample obtained from the absorbance spectra.

### 3. XPS

The ceria surface stoichiometry for the CeO<sub>2</sub> film and Ag@CeO<sub>2</sub> sample was evaluated by fitting Ce 3d XPS spectra using Ce<sup>3+</sup>- and Ce<sup>4+</sup>-related components, following Skala et al.<sup>3</sup> The Ce 3d spectra of the two samples and the fitting curves are shown in Figure S4. The concentration of Ce<sup>3+</sup> in the Ag@CeO<sub>2</sub> sample is 9 % while the concentration of Ce<sup>3+</sup> in the 10 nm CeO<sub>2</sub> film, is 5%, giving a stoichiometry close to CeO<sub>2</sub> for both samples.

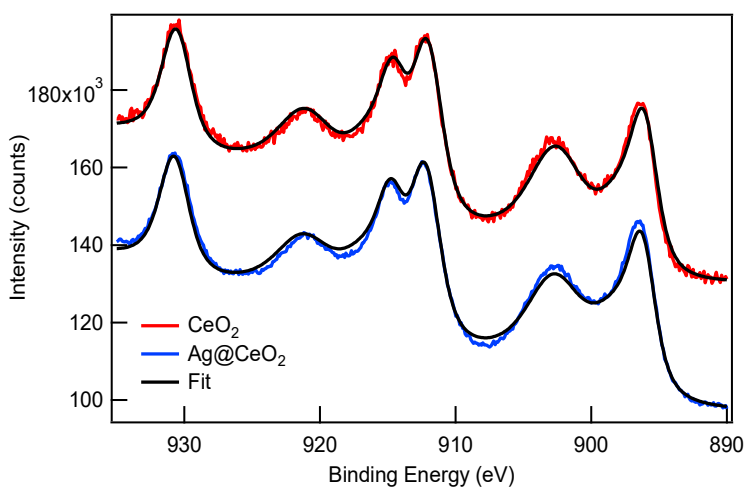


**Figure S4.** Ce 3d XPS spectra of the 10 nm CeO<sub>2</sub> film (red line) and the Ag@CeO<sub>2</sub> sample (blue line). The black lines are the fits of the spectra using Ce<sup>3+</sup> and Ce<sup>4+</sup> related components.

### 4. Boundary element simulations

In order to explain the double plasmon resonance peak originating from the Ag NPs, we performed calculations using the MNPBEM, a toolbox developed by Hohenester and coworkers.<sup>4</sup> This computational instrument is based on the boundary element method (BEM) approach developed by Garcia de Abajo and A. Howie<sup>5</sup> and it allows calculation of the absorption, scattering and extinction coefficients of metal NPs embedded in and sitting on dielectric materials. The dielectric constants for the specific photon energies were obtained from tabulated *n* and *k* values obtained by Palik (Ag)<sup>6</sup> and Kim (CeO<sub>2</sub>).<sup>7</sup> Different geometries were implemented including nanorods, spheroids and ellipsoidal

nanodisks (Figure S5). The geometry which provides the best agreement with the experimental data is a spheroid with axis lengths of 10, 10 and 15 nm, in good agreement with the Ag nanoparticle size and shape determined from the STEM images. The calculated absorption coefficients for this geometry (Figure S5a) show two peaks at 450 and 600 nm due to the transverse (polarization perpendicular to the major axis of the ellipsoid) and longitudinal (polarization parallel to the major axis of the ellipsoid) LSPRs. We simulated also Ag nanodisks supported on top of a CeO<sub>2</sub> film. The calculated absorption spectrum in this case (Figure S5 c) shows a much worse agreement with the experimental spectrum. The same nanodisk embedded within a CeO<sub>2</sub> film gives a simulated spectrum (Figure S5 b) compatible with the experimental one, though the ellipsoidal NP gives a better agreement in terms of wavelengths of absorbance maxima.

The plasmonic feature at higher wavelengths compared to the dominant resonance may also originate from a collective plasmonic resonance, involving two or more NPs with mutual distance of the order of a few nm.<sup>8</sup> For two adjacent metallic spheres a lower-energy resonance is generated by two longitudinally aligned dipoles and it gives rise to a strongly red-shifted absorption peak in the optical spectrum.<sup>9</sup> To test this hypothesis, we performed some BEM simulations of two NPs with 10 nm

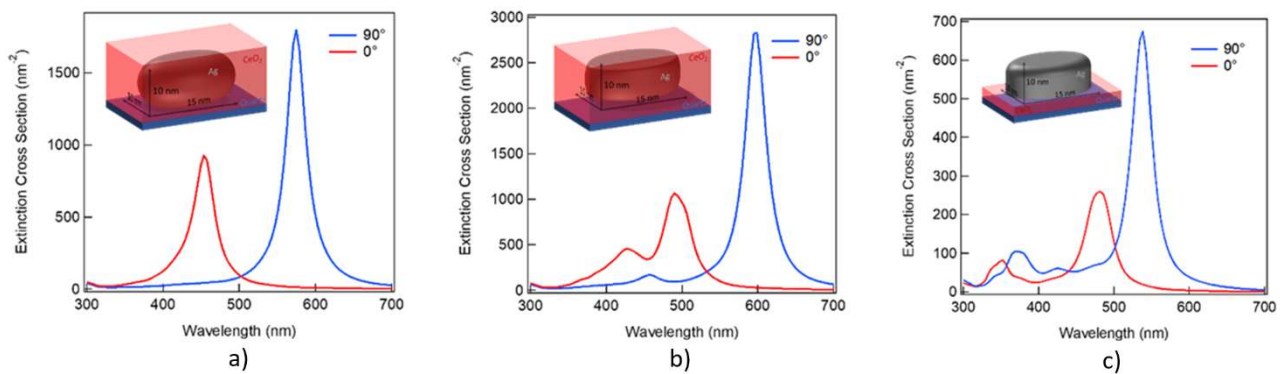


**Figure S5.** Simulated extinction cross section spectra obtained using the MNPBEM toolbox<sup>3</sup> with a linearly polarized light parallel (red curves) and perpendicular (blue curves) to the minor axis of a) embedded ellipsoidal NP with geometry [15 10 10] nm in a 10 nm ceria film, b) nanodisk with geometry [15 10 10] nm embedded in 15 nm of ceria and c) the same nanodisk supported over 10 nm film of ceria.

diameter embedded in 11 nm of ceria using variable distances from 0.5 to 3.5 nm. The results, reported in Figure S6, show that the interparticle distance needs to be smaller than 2 nm to obtain a

peak with a wavelength above 550 nm (Figure S6). In our sample the equivalent thickness of the Ag NP layer - 5 nm, i.e. one half of a closed layer - is not compatible with such a small interparticle distance. If, for example, we hypothesize a hexagonal packing at a similar coverage, we obtain a distance between the NPs of 3.5 nm. We therefore consider unlikely for collective plasmonic resonances to significantly contribute to the absorbance peak at 550 nm.

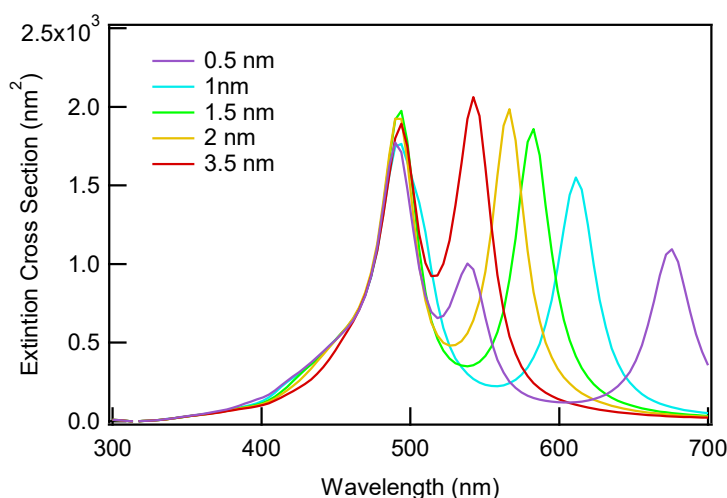


**Figure S6.** BEM simulation of two spherical NPs with diameter of 10 nm embedded in 11 nm of CeO<sub>2</sub> with different distances between the two surfaces.

## 5. Transient absorbance spectra at short delay times

At short delay times between the pump and the probe the Ag@CeO<sub>2</sub> transient absorbance (TA) spectra pumped above (Figure S7a) and below (Figure S7b) the ceria bandgap are dominated in the visible region by the plasmonic transient signals. These include a negative bleaching in the region 380-520 nm and two positive features at 610 nm and 350 nm. The positive wing at low wavelength overlaps with the ceria-related signal at 345 nm, hindering the possibility to extract an injection time for the electrons transferred to Ce 4f levels.

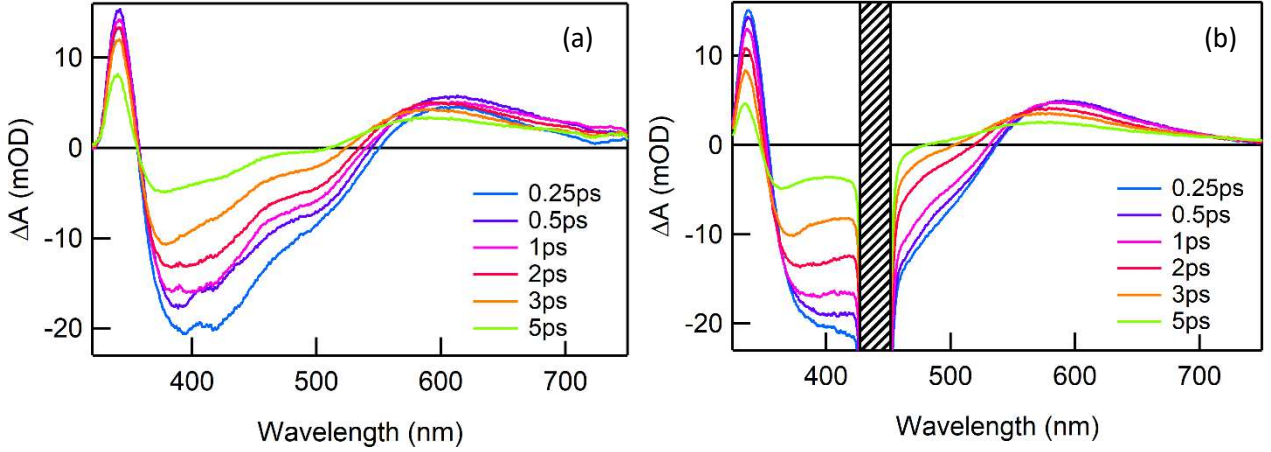


**Figure S7.** TA spectra of the Ag@CeO<sub>2</sub> sample with (a) 275 nm pump and (b) 440 nm pump and visible probe at delay times below 5 ps.

## 6. Fit of the time evolution of the photoinduced absorption signal

In Figure 6 of the main text we compare the time evolution of the photoinduced absorption signal in the different samples, excited at the different pump energies, by considering horizontal cuts of the TA maps at 345 nm.

The fitting of the curve for the CeO<sub>2</sub> sample was performed by a linear combination of a rising function at ultrashort times and an exponentially decreasing function at longer times, convolved with a Gaussian kernel which represents the instrument response function (IRF) estimated as 0.05 ps:

$$f_{CeO_2}(t) = T_{CeO_2}(t) + A_0 = A_1 \cdot \left(1 + \operatorname{erf}\left(\frac{c+t}{IRF}\right)\right) - A_1 \cdot e^{-\frac{c-t}{\tau_1}} \cdot e^{-\frac{IR^2}{4\tau_1^2}} \cdot \left(1 + \operatorname{erf}\left(\frac{c+t}{IRF} - \frac{IRF}{2\tau_1}\right)\right) + A_2 \cdot e^{-\frac{c-t}{\tau_2}} \cdot e^{-\frac{IRF^2}{4\tau_2^2}} \cdot \left(1 + \operatorname{erf}\left(\frac{c+t}{IRF} - \frac{IRF}{2\tau_2}\right)\right) + A_0$$

with  $A_0$ ,  $A_1$ ,  $A_2$ ,  $\tau_1$ ,  $\tau_2$ ,  $c$  as free fitting coefficients.

A linear combination of the  $T_{CeO_2}$  function, with fixed  $A_1$ ,  $A_2$ ,  $\tau_1$ ,  $\tau_2$ , and  $c$  as obtained from the fitting of the CeO<sub>2</sub> sample decay, and an additional exponentially decreasing function at short times, describing plasmonic decay, was used to fit the Ag@CeO<sub>2</sub> signal at the different pump energies:

$$f_{Ag@CeO_2}(t) = G * T_{CeO_2}(t) + A_3 \cdot e^{-\frac{c-t}{\tau_3}} \cdot e^{-\frac{IRF^2}{4\tau_3^2}} \cdot \left(1 + \operatorname{erf}\left(\frac{c+t}{IRF} - \frac{IRF}{2\tau_3}\right)\right) + A_0$$

The coefficients which gave the best fit for the different samples and the different pump energies are summarized in Table S1.

parameter \ sample	A <sub>0</sub> (mOD)	A <sub>1</sub> (mOD)	A <sub>2</sub> (mOD)	A <sub>3</sub> (mOD)	τ <sub>1</sub> (ps)	τ <sub>2</sub> (ps)	τ <sub>3</sub> (ps)	c (ps)	G
<b>CeO<sub>2</sub></b>	0.2 ± 0.3	3.1 ± 0.2	1.9 ± 0.3	-	0.8 ± 0.1	60 ± 20	-	0.18 ± 0.01	-
<b>Ag@CeO<sub>2</sub></b>	1.0 ±	3.1	1.9	8.3 ±	0.8	60	2.9 ±	0.03 ±	0.53 ±
<b>pump 275 nm</b>	1.1	fixed	fixed	0.3	fixed	fixed	0.2	0.01	0.08
<b>Ag@CeO<sub>2</sub></b>	0.7 ±	3.1	1.89	6.8 ±	0.8	60	2.3 ±	0.006 ±	0.09 ±
<b>pump 440 nm</b>	0.2	fixed	fixed	0.2	fixed	fixed	0.1	0.004	0.04

**Table S1.** Parameters obtained from the fitting of the time evolution of the photoinduced absorption signal.

## 7. Injection efficiency evaluation

Figure 7a of the main text reports the density of electrons injected in the 4f levels (proportional to  $\Delta A(t) \cdot t$  in the temporal range [50;250] ps) as a function of the incident photon density at the different pump fluences and energies. The proportionality constant  $\kappa$  obtained from the linear fits of the data using formula (S1), fixing the intercept to 0 mOD·ps and using the error on the fluence as the weight of the fit, are reported in Table S2.

$$\Delta A \cdot t = \kappa N_{phot} \quad (S1)$$

Sample	Pump wavelength (nm)	$1/\kappa$ (mOD <sup>-1</sup> ps <sup>-1</sup> cm <sup>-2</sup> )
CeO <sub>2</sub>	275	$(49 \pm 9) 10^{15}$
Ag@ CeO <sub>2</sub>	275	$(46 \pm 8) 10^{15}$
Ag@ CeO <sub>2</sub>	410	$(33 \pm 10) 10^{16}$
Ag@ CeO <sub>2</sub>	440	$(32 \pm 7) 10^{16}$
Ag@ CeO <sub>2</sub>	475	$(4.1 \pm 1.2) 10^{17}$
Ag@ CeO <sub>2</sub>	510	$(3.0 \pm 1.1) 10^{17}$
Ag@ CeO <sub>2</sub>	600	$(8 \pm 3) 10^{17}$

**Table S2.**  $1/\kappa$  values obtained for different pump energies.

## Bibliography

1. S. D'Addato, D. Pinotti, M. C. Spadaro, G. Paolicelli, V. Grillo, S. Valeri, L. Pasquali, L. Bergamini and S. Corni, *Beilstein Journal of Nanotechnology*, 2015, **6**, 404-413.
2. V. Grillo and E. Rotunno, *Ultramicroscopy*, 2013, **125**, 97-111.
3. T. Skála, F. Šutara, M. Škoda, K. C. Prince and V. Matolín, *Journal of Physics: Condensed Matter*, 2009, **21**, 055005.
4. U. Hohenester and A. Trügler, *Computer Physics Communications*, 2012, **183**, 370-381.
5. F. J. García de Abajo and A. Howie, *Phys Rev B*, 2002, **65**, 115418.
6. J. Barth, R. Johnson and M. Cardona, *Handbook of Optical Constants of Solids II*, Academic Press, New York, 1991.
7. W.-H. Kim, W. J. Maeng, M.-K. Kim, J. Gatineau and H. Kim, *Journal of The Electrochemical Society*, 2011, **158**, G217-G220.
8. H. Cha, D. Lee, J. H. Yoon and S. Yoon, *Journal of Colloid and Interface Science*, 2016, **464**, 18-24.
9. F. Chen, N. Alemu and R. L. Johnston, *AIP Advances*, 2011, **1**, 032134.